J. Biochem. **138**, 263–275 (2005)
DOI: 10.1093/jb/mvi120

Novel Reaction Mechanism of GTP Cyclohydrolase I. High-Resolution X-Ray Crystallography of *Thermus thermophilus* HB8 Enzyme Complexed with a Transition State Analogue, the 8-Oxoguanine Derivative

Yoko Tanaka[1], Noriko Nakagawa[1,2], Seiki Kuramitsu[1,2,3], Shigeyuki Yokoyama[2,3,4] and Ryoji Masui[1,2,*]

[1]Department of Biology, Graduate School of Science, Osaka University, 1-1 Machikaneyama-cho, Toyonaka, Osaka 560-0043; [2]RIKEN Harima Institute at SPring-8, 1-1-1 Kouto, Mikazuki-cho, Sayo-gun, Hyogo 679-5148; [3]RIKEN Genomic Sciences Center, 1-7-22 Suehiro-cho, Tsurumi, Yokohama 230-0045; and [4]Department of Biophysics and Biochemistry, Graduate School of Science, The University of Tokyo, 7-3-1 Hongo, Bunkyo-ku, Tokyo 113-0033

Received May 7, 2005; accepted June 2, 2005

GTP cyclohydrolase I (GTPCH1) catalyzes the conversion of GTP to dihydroneopterin 3′-triphosphate. We found that an 8-oxoguanine derivative of GTP (8-oxo-GTP) strongly bound to GTPCH1 from *Thermus thermophilus* HB8 (tGTPCH1) as a competitive inhibitor. The affinity of 8-oxo-GTP was three orders of magnitude greater than that of GTP. These results suggest that 8-oxo-GTP is a transition state analogue of GTPCH1. We have solved the X-ray crystal structures of tGTPCH1 complexed with 8-oxo-GTP and 8-oxo-dGTP at 2.0 and 1.8 Å resolution, respectively, as well as the free form of the enzyme at 2.2 Å resolution. In the structure of tGTPCH1 complexed with 8-oxo-GTP or 8-oxo-dGTP, the oxygen atoms at O8 of the 8-oxoguanine groups, together with residues Cys108, His111 and Cys179, are coordinated to the zinc ion. The water molecule between Nδ1 of His177 and N7 of 8-oxoguanine is conserved in both structures. These structural data are in accordance with one of the proposed transition states. Superimpositioning of the structures indicates the imidazole ring of His110 is rotated, implying concomitant proton transfer to the ribose ring O4′. Based on these structural data we propose a novel reaction mechanism for GTPCH1.

Key words: GTP cyclohydrolase I, 8-oxoguanine, *Thermus thermophilus* HB8, transition state analogue, zinc enzyme.

Abbreviations: AFRPT, 2-amino-5-formylamino-(6β)-ribosylamino-4(3*H*)-pyrimidinone 5′-triphosphate; BH_4, tetrahydrobiopterin; DRPT, 2,5-diamino-(6β)-ribosylamino-4(3*H*)-pyrimidinone 5′-triphosphate; FapyG, 2,6-diamino-4-hydroxy-5-formamidopyrimidine; GTPCH1, GTP cyclohydrolase I; eGTPCH1, GTPCH1 from *Escherichia coli*; hGTPCH1, GTPCH1 from man; rGTPCH1, GTPCH1 from rat; tGTPCH1, GTPCH1 from *Thermus thermophilus* HB8; NH_2TP, dihydroneopterin 3′-triphosphate; and 8-oxo-GTP (8-oxo-dGTP), (d)GTP containing an oxidatively damaged form of guanine (7,8-dihydro-8-oxoguanine).

GTP cyclohydrolase I (GTPCH1) [EC 3.5.4.16] is a key enzyme in the biosynthesis of several cofactors [*e.g.*, folic acid in bacteria and tetrahydrobiopterin (BH_4) in mammalian species]. The common reaction step in these biosynthetic pathways is the formation of dihydroneopterin triphosphate (NH_2TP, 6-D-threo-1′,2′,3′-hydroxypropyl-7,8-dihydroneopterin 3′-triphosphate) from GTP (Fig. 1). This complex reaction comprises several steps: purine base opening, formic acid release, ribose ring opening and rearrangement of the carbohydrate side chain, followed by formation of the pyrazine ring of the product. Moreover, conformational reorientation of the reactant appears to be required in the ring closure step. Among the reaction intermediates shown in Fig. 1, 2-amino-5-formylamino-(6β)-ribosylamino-4(3*H*)-pyrimidinone 5′-triphosphate (AFRPT) was identified experimentally (*1*, *2*), whilst 2,5-diamino-(6β)-ribosylamino-4(3*H*)-pyrimidinone 5′-triphosphate (DRPT) was proposed (*3*).

GTPCH1 was partially purified and named by Burg and Brown (*3*) over 30 years ago. The proposed reaction mechanism of GTPCH1 involved non-enzymatic Amadori rearrangement. Although evidence for the participation of Amadori rearrangement was provided (*4*, *5*), refinement of the proposed reaction mechanism has had to await structural analysis of the enzyme. The major biochemical properties of GTPCH1s purified from various species have been studied, including the pH dependence of their activity. However, identification of functional groups of GTPCH1 has been problematic, due in part to the instability of the enzyme.

Nar *et al.* (*6*) first solved the structure of free GTPCH1 from *Escherichia coli* (eGTPCH1) in the absence of coordinated zinc. Five years later, the zinc coordinated structures were solved for eGTPCH1 as well as human GTPCH1 (hGTPCH1) (*7*). These GTPCH1s exhibit 5-fold symmetry with a central β-barrel sandwiched by α-helices. The active site is made up of three adjacent subunits. The zinc ion in the active site is coordinated to one His and two Cys residues. Mutation of these residues resulted in loss of activity (*8*). Rebelo *et al.* (*9*) solved the

*To whom correspondence should be addressed. E-mail: rmasui@bio.sci.osaka-u.ac.jp

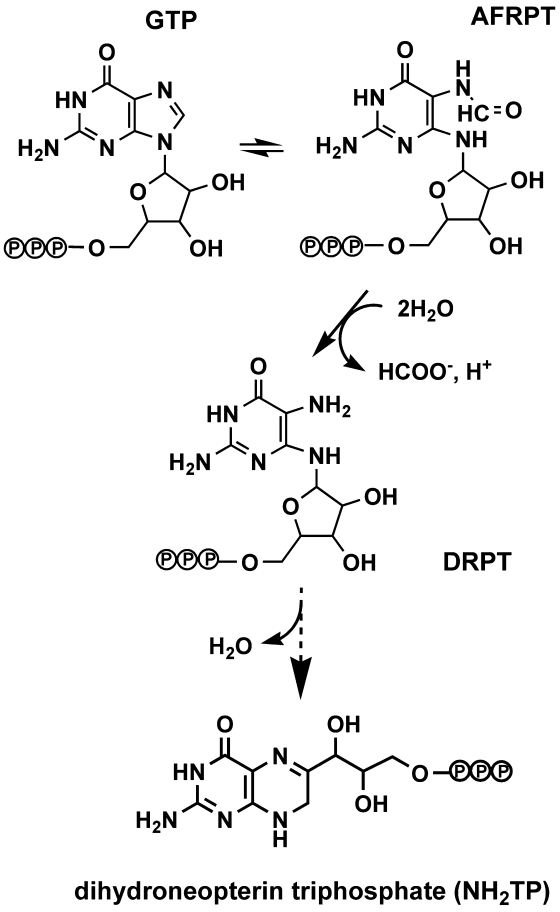

Fig. 1. **Current model of the mechanism of GTPCH1 activity.**

three mutant structures of eGTPCH1 complexed with GTP and proposed a reaction mechanism. According to their hypothesis, His112 (eGTPCH1) participates in the two bond-cleavage steps and the zinc ion participates in the release of formic acid through coordination to its two oxygen atoms. Until now, however, the structure of wild-type GTPCH1 complexed with zinc and a substrate or analogue had not been solved.

The thermostable properties of proteins from *T. thermophilus* HB8 (*10*) make them particularly suitable for structural and functional analyses (*11*). In general, these proteins can be easily crystallized and often give high-resolution diffraction data. In this paper, we report that tGTPCH1 exhibited high affinity for the 8-oxoguanine derivative of GTP (8-oxo-GTP). The results of structural analyses, as well as the affinity data, suggest that 8-oxo-GTP is a transition state analogue of GTPCH1. The high-resolution data also suggest the participation of a zinc ion and water molecules in the transition state. From these results a new reaction mechanism for tGTPCH1 is proposed. The possible physiological meaning of the high affinity of 8-oxo-GTP is also discussed.

MATERIALS AND METHODS

Materials—8-Oxo-GTP and 8-oxo-dGTP were purchased from TriLink BioTechnologies. Neopterin, isopropyl β-D-thiogalactopyranoside and phenylmethylsulfonyl fluoride were from Wako Pure Chemicals. Restriction enzymes were from Takara-Bio Inc. and New England Biolabs.

Cloning and Overexpression—The gene for GTPCH1 was amplified by the polymerase chain reaction using the following primers: 5′-ATATCATATGAGCCCGGGGCCA-CAGAGCGGGGGGC-3′ and 5′-ATATAGATCTTTATTA-GGCCGTCCCGT-CCCTGAGGTGGCTC-3′. The amplified product was cloned into plasmid pT7Blue (Novagen). After confirmation of the nucleotide sequence, the plasmid was digested with *Nde*I and *Bgl*II. The resulting DNA fragment containing the gene was inserted between the *Nde*I and *Bam*HI sites in pET-11a (Novagen). The expression plasmid was used to transform *E. coli* strain BL21(DE3) (Novagen). Transformants were cultured by the high-cell density method at 37°C in 3 liters of 2× YT (tryptone-yeast extract-rich) medium containing ampicillin (50 μg ml^{-1}). Cultivation was performed under 0.1 MPa until the *E. coli* growth had reached the plateau of 5 × 10^9/ml. Cultivation was then continued under higher pressure (0.12 MPa) for 36 h until the cell density reached 1–2 × 10^{11}/ml. During cultivation approximately 1 liter of 2 N NaOH was added automatically to maintain the pH value of the medium at a neutral level (pH 7.2). Nutrient demand was met by adding glucose (300 g). Heterologous gene expression was then induced by adding isopropyl β-D-thiogalactopyranoside (50 μg ml^{-1}). After continuing the cultivation for 5 h, the cells (125 g) were harvested and stored at –20°C.

Protein Purification—All operations were carried out at 4°C unless stated otherwise. About 25 g of frozen cells was thawed and suspended in 50 mM Tris-HCl (pH 7.5), 10 mM 2-mercaptoethanol and 1 mM phenylmethylsulfonyl fluoride. After disruption of the cells by sonication, the lysate was centrifuged at 30,000 × *g* for 60 min. The supernatant was heated at 70°C for 20 min, chilled on ice and then centrifuged at 30,000 × *g* for 60 min. The resulting supernatant was applied to a Toyopearl SuperQ-650M column (Tosoh) equilibrated with 50 mM Tris-HCl (pH 7.5) and 10 mM 2-mercaptoethanol at 4°C. Protein was eluted with a linear KCl gradient (0–1 M). Target fractions were collected, diluted with an equal volume of 50 mM Tris-HCl (pH 7.5), 10 mM 2-mercaptoethanol and 60% ammonium sulfate, and then applied to a Toyopearl Butyl-650M column (Tosoh) equilibrated with 50 mM Tris-HCl (pH 7.5), 10 mM 2-mercaptoethanol and 30% ammonium sulfate. Protein fractions were eluted with a linear ammonium sulfate gradient (30–0%) at 4°C. The collected fractions were dialyzed overnight against 20 mM Tris-HCl (pH 7.5) and 10 mM 2-mercaptoethanol. Protein was concentrated with a Vivaspin spin concentrator (molecular mass cut-off, 10,000 Da) (Viva Science) and then applied to a MonoQ column (Amersham Biosciences) equilibrated with 20 mM Tris-HCl (pH 7.5). GTPCH1 was eluted with a linear gradient of KCl (0–1 M). The tGTPCH1 peak fractions were collected and concentrated.

Enzyme Assay—Enzyme assays were performed by the method of Fukushima *et al.* (*12*) with slight modification. The reaction mixture comprised 50 mM Tris-HCl (pH 8.5), 0.1 M KCl, the desired concentration of GTP and about 0.2 μM enzyme. Reactions were performed at 25°C

Table 1. **Data collection and refinement statistics.**

Data set	Free	Complex with 8-oxo-GTP	Complex with 8-oxo-dGTP
Data collection			
Beamline	BL45PX/SPring-8	BL45PX/SPring-8	BL45PX/SPring-8
Unit-cell parameters			
a (Å)	160.22	160.20	160.53
b (Å)	110.48	110.96	110.59
c (Å)	70.65	70.46	70.65
β (°)	105.27	105.53	105.81
Space group	*C*2	*C*2	*C*2
Resolution (Å)[a]	50–2.2 (2.28–2.20)	50–2.0 (2.07–2.00)	50–1.8 (1.89–1.82)
Wavelength (Å)	1.0	1.0	0.98
Observations (No.)	196,546	290,012	233,632
Unique reflections (No.)	58,232	79,691	103,478
Data completeness (%)	96.6 (94.1)	99.1 (99.6)	98.5 (98.7)
R_{merge}[b]	0.067 (0.292)	0.054 (0.251)	0.050 (0.297)
Average I/σ	22.4 (4.3)	27.3 (5.6)	25.0 (3.4)
Refinement statistics			
Resolution limits (Å)	50–2.2	50–2.0	50–1.8
R_{cryst}[c]	0.208	0.2066	0.2052
R_{free}[d]	0.261	0.2367	0.2358
Average B factor (Å^2)	33.7	34.1	25.5
R.m.s. deviation from ideality			
Bond length (Å)	0.006	0.006	0.006
Angles (°)	1.35	1.36	1.33
Dihedral angles (°)	23.52	22.85	22.86
Improper angles (°)	1.17	1.19	1.16

[a]Values in parentheses are for the outermost shell of data. [b]$R_{merge} = \Sigma |I_{obs} - \langle I \rangle| / \Sigma I_{obs}$. [c]$R_{cryst} = \Sigma ||F_{obs}| - |F_{calc}|| / \Sigma |F_{obs}|$. [d]$R_{free}$ is monitored with 10% of the reflection data excluded from refinement.

for 60–180 min and terminated by the addition of an iodine solution comprising 1% iodine and 2% KI in 1 N HCl. The product (NH_2TP) was oxidized to neopterin triphosphate by the iodine. Excess iodine was reduced by the addition of 2% ascorbic acid. 1 N NaOH and 1 M Tris-HCl (pH 8.0) were added to neutralize the reaction mixture. The fluorescence of neopterin triphosphate was measured with excitation at 355 nm and emission at 460 nm using a Hitachi spectrofluorimeter, model F-4500. Since the triphosphate moiety of NH_2TP was not fluorescent, the fluorescent intensity of neopterin was assumed to be the same as that of NH_2TP (*13*).

Kinetic Studies—Steady-state kinetic parameters were analyzed with GTP or GDP as the substrate. K_m and k_{cat} were calculated with the Michaelis-Menten equation using the curve fitting software Igor Pro (WaveMetrics). For pH profile experiments, the reaction mixture comprised 0.5 mM GTP, 50 mM buffer component and 0.1 M KCl.

Competitive inhibition of ATP, dGTP, 8-oxo-dGTP or 8-oxo-GTP was studied. In the case of the 8-oxoguanine derivatives, the affinities were rather high, and the concentrations of the inhibitors and the enzyme were comparable, and thus correction for enzyme concentration was necessary to calculate the inhibition constants (*14*, *15*). In the presence of both GTP and 8-oxo-GTP, GTPCH1 is inhibited in a competitive manner. Only ES can produce NH_2TP.

$$[E]_0 = [E] + [ES] + [EI] \quad (1)$$

$$[S]_0 = [S] + [ES] \quad (2)$$

$$[I]_0 = [I] + [EI] \quad (3)$$

$$K_m = [E][S]/[ES] \quad (4)$$

$$K_i = [E][I]/[EI] \quad (5)$$

Based on Eqs. 1–5, [ES] at the desired GTP concentration is obtained by solving Eq. 6.

$$\begin{aligned} f([ES]) = {} & (K_m - K_i)[ES]^3 + \{-(K_m - K_i)([E]_0 + [S]_0 + K_m) \\ & + K_i[S]_0 + K_m[I]\}[ES]^2 + [S]_0\{[E]_0(K_m - 2K_i) \\ & - [S]_0K_i - [I]_0K_m - K_mK_i\}[ES] + [E]_0[S]_0^2K_i = 0 \end{aligned} \quad (6)$$

$$v = k_{cat}[ES]$$

From v-[S] plots, K_i is obtained.

To determine the concentration of the inhibitory complex with 8-oxoguanine derivatives, we introduce α, *i.e.*, the ratio of intact enzyme-substrate complex to total enzyme complex.

$$\alpha = [ES]/([ES] + [EI]) \quad (7)$$

From Eqs. 1–7,

$$\begin{aligned} f([ES]) = {} & [ES]^3 + \{([S]_0 + [I]_0) + 2[E]_0 + K_m + K_i\}[ES]^2 \\ & + \{([S]_0 + [I]_0 + 1)(2[E]_0 + K_m + K_i) \\ & + ([E]_0 + K_m)([E]_0 + K_i) - (K_m[S]_0 + K_i[I]_0)\}[ES] \\ & + K_m[S]_0([E]_0 + K_i) + K_i[I]_0([E]_0 + K_m) \\ & - ([S]_0 + [I]_0)([E]_0 + K_m)([E]_0 + K_i) = 0 \end{aligned} \quad (8)$$

$$\alpha = [S]_0([E]_0 - [ES])/[ES](K_m + [E]_0 - [ES]) \quad (9)$$

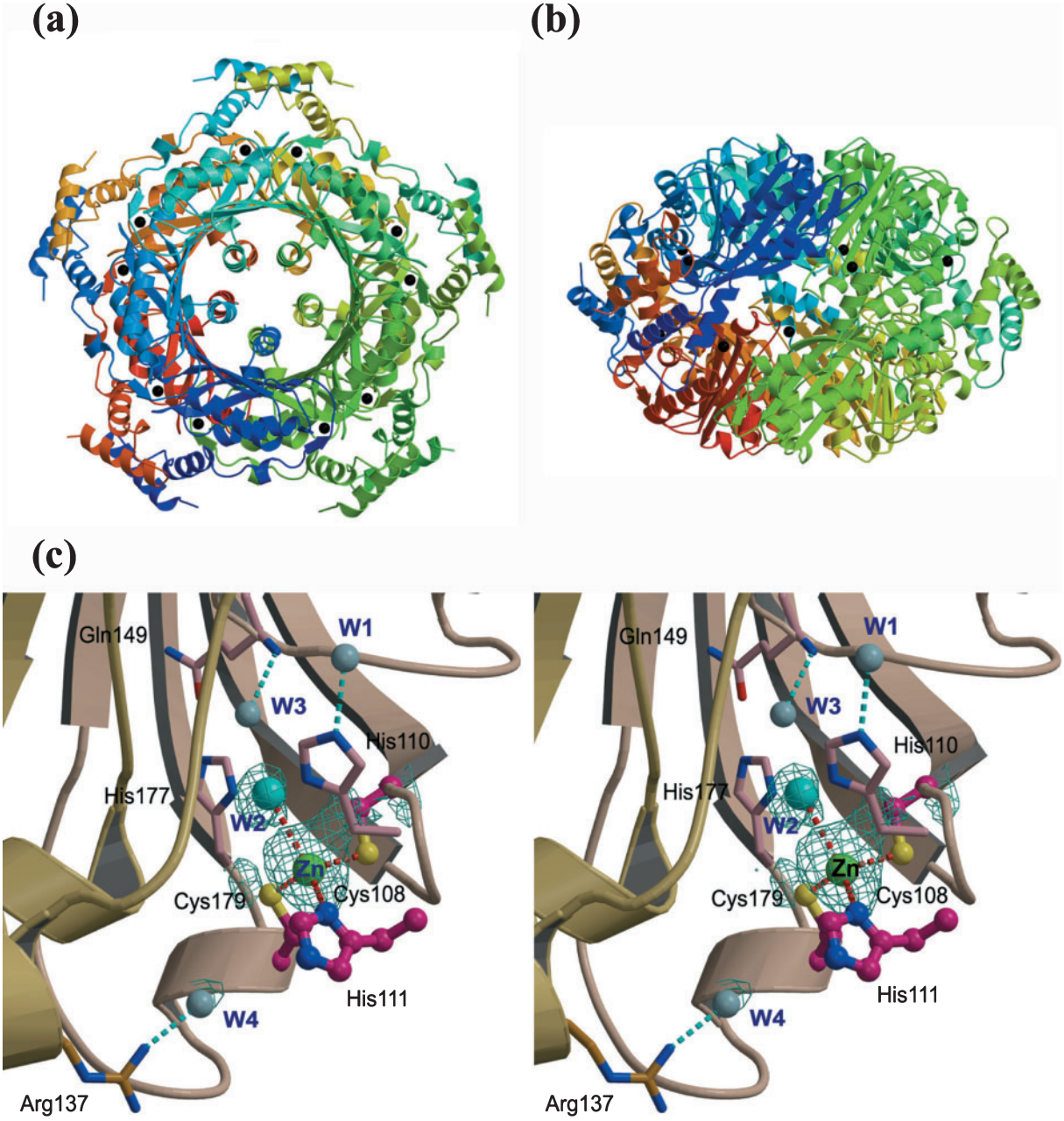

Fig. 2. **Overall structure of free tGTPCH1.** (a, b) Top and side views of the decameric structure of free tGTPCH1. Each subunit in ribbon form is differently colored. Black balls represent the zinc ions at the active sites. (c) Enlarged stereo view of the active site of free tGTPCH1. The zinc ion (green) and water molecules (cyan or gray) are shown as balls. The difference Fourier map ($1F_o - F_c$ map, σ = 3.0) is superimposed on the model. Residues coordinated to Zn are drawn as ball-and-stick models, whereas other residues are drawn as stick models.

Substituting $[E]_0$ = 16 nM, $[S]_0$ = 150 μM, K_m = 4.2 μM and K_i = 0.0054 μM in Eq. 8, solving of f([ES]) = 0, [ES] was possible. From Eq. 9, α was calculated with various 8-oxoguanine/guanine ratios.

Crystallization—Initial screening for tGTPCH1 crystallization conditions was performed using the hanging-drop vapor-diffusion method at 20°C and a Crystal Screen Cryo (Hampton Research). The initial protein concentration was 13.7 mg/ml. Drops were prepared by mixing 2 μl of protein solution with 2 μl reservoir solution, and equilibrated against 200 μl of reservoir solution. The free form of tGTPCH1 was crystallized with the following reservoir solutions: 0.1 M HEPES (pH 6.8), 2.0 M ammonium sulfate, 3.4% polyethyleneglycol (PEG) 400, and 15% glycerol. Crystals of tGTPCH1 complexed with an 8-oxoguanine derivative were obtained by co-crystallization with 1 mM 8-oxo-GTP or 10 mM 8-oxo-dGTP. The crystallization conditions were the same as those used for the free form except for the glycerol content (25% instead of 15%).

X-Ray Diffraction Data Collection and Refinement—X-ray diffraction data for crystals were collected with a

mosaic CCD detector (Jupiter 210, Rigaku) at –163°C, using synchrotron radiation at SPring-8 beam line BL45XU-PX. Crystals were prepared under cryo resistant conditions, so no extra cryoprotectant was needed. The data processing was completed using HKL2000 (*16*). The space group of all crystals was *C*2 and each of the unit cell parameters was about the same (Table 1). To determine the structure of the free protein we employed the molecular replacement method, using the pentamer of hGTPCH1 (*7*) as a model molecule (PDB code; 1FB1). The AMORE program (*17*) was used in the resolution range of 15.0 to 4.0 Å with an integration vector of 20 Å. The highest solution found exhibited 5-fold symmetry, a correlation coefficient of 0.637 and an *R* factor of 44.7%. Manual model building and subsequent iterative refinement were performed using the O and CNS programs, respectively. The same refinement procedure was applied to the structures of the two complexes with 8-oxo-dGTP and 8-oxo-GTP, except that the coordinates of free tGTPCH1 and tGTPCH1 in complex with 8-oxo-dGTP were used as the initial model, respectively. All protein crystals have one region of high electron density in the active site per subunit. This density was assigned to a zinc ion on measurement of the X-ray absorption fine structure. No other regions of high electron density were observed. The structures of free tGTPCH1, and tGTPCH1 in complexes with 8-oxo-dGTP and 8-oxo-GTP were refined at 2.2, 1.8 and 2.0 Å resolution, respectively. A summary of the refinement statistics for all structures is presented in Table 1. A symmetrical operation and superimpositioning of this pentamer resulted in the decamer structure (Fig. 2, a and b). The decamer structure was also confirmed in an aqueous solution (data not shown).

Graphics—Figures were prepared using Molscript (*18*) and Raster3D (*19*). The homology picture was drawn with ESPript (*20*). The hydrogen bonding network diagram was drawn with LIGPLOT (*21*).

Protein Data Bank Accession Code—The atomic coordinates of free tGTPCH1, and tGTPCH1 in complexes with 8-oxo-GTP and 8-oxo-dGTP have been deposited in the PDB under the accession codes 1WM9, 1WUQ and 1WUR, respectively.

RESULTS

Steady-State Kinetics of tGTPCH1—tGTPCH1 was overproduced in *E. coli* cells and then the recombinant protein was purified to homogeneity by column chromatography in three steps (see "MATERIALS AND METHODS"). tGTPCH1 activity was assayed under steady-state conditions. The NH_2TP production kinetics followed the Michaelis-Menten equation, and K_m and k_{cat} were calculated. For GTP, k_{cat} = 0.0035 s^{-1}, K_m = 4.2 μM at 25°C (Table 2), k_{cat} = 0.053 s^{-1}, K_m = 12.8 μM at 60°C, and k_{cat} = 0.14 s^{-1}, K_m = 20.8 μM at 75°C. From these results, ΔG = –9.7 kcal/mol, ΔH = –6.6 kcal/mol, $T\Delta S$ = 3.1 kcal/mol, $\Delta G^{\ddagger}$ = 21.5 kcal/mol, $\Delta H^{\ddagger}$ = 15.8 kcal/mol, and $T\Delta S^{\ddagger}$ = –5.6 kcal/mol at 25°C were obtained (*22*). For the binding step (ΔH = –6.6 kcal/mol and $T\Delta S$ = 3.1 kcal/mol), substrate-binding and water-release processes might compensate for each other. Bond cleavage may be the rate-limiting step ($\Delta H^{\ddagger}$ = 15.8 kcal/mol and $T\Delta S^{\ddagger}$ = –5.6 kcal/mol).

Table 2. **Kinetic parameters of tGTPCH1.**

Substrate or inhibitor	k_{cat} (s^{-1})	K_m or K_i (μM)	ΔG_u[a] (kcal mol^{-1})
GTP	0.0035	4.2	–9.7
GDP	0.0017	143	–7.6
dGTP	0	20	–8.8
ATP	0	71	–8.1
8-oxo-GTP	0	0.0054	–13.7
8-oxo-dGTP	0	0.22	–11.5

[a]ΔG_u: unitary free energy, ionic strength 0.1, pH 8.5, 25°C.

These results are similar to those obtained for other GTPCH1s isolated from various organisms (*23–28*) suggesting they share an identical reaction mechanism.

In addition to GTP, tGTPCH1 also catalyzed the reaction from GDP with K_m = 142 μM and k_{cat} = 0.0017 s^{-1}. dGTP and ATP acted as competitive inhibitors with K_i values of 20 and 71 μM, respectively. GMP showed neither reaction nor inhibition, even at 1 mM (Table 2). When a substrate analogue, dGTP, 8-oxo-GTP or 8-oxo-dGTP, was incubated with tGTPCH1, HPLC analysis gave only a peak corresponding to each triphosphate, indicating that these compounds do not act as substrates for the enzyme. Surprisingly, 8-oxo-GTP and 8-oxo-dGTP inhibited tGTPCH1 in a competitive manner with inhibition constants of 0.0054 and 0.22 μM, respectively, which are much smaller than K_i for dGTP (20 μM) and K_m for GTP (4.2 μM) (Table 2). The unitary free energy (ΔG_u) of a substrate or analogue was calculated from K_m or K_i using the following equation: $\Delta G_u = -RT \ln K - 2.39$. The results are listed in Table 2.

Sequence Homology—Figure 3 shows multiple amino acid sequence alignment of GTPCH1s from prokaryotes to man. Except for the N-terminal region, significant homology was found throughout the length of the polypeptide. In mammals, rat GTPCH1 (rGTPCH1) and hGTPCH1 exhibit a high level of homology over the entire sequence. The residues forming the ligand-binding pocket (Fig. 3, indicated by triangles) are highly conserved. The zinc coordinating residues and the catalytic residues are all conserved. tGTPCH1 exhibited 36% homology to eGTPCH1, and 58% homology to hGTPCH1 and rGTPCH1.

The contents of charged residues (Asp, Glu, His, Arg and Lys) were 29.1% in tGTPCH1, 24.9% in eGTPCH1 (*7*), 25.3% in hGTPCH1 (*7*), and 25.8% in rGTPCH1 (*29*). This seems to be consistent with the tendency of proteins from thermophiles to have high ion pair contents (*30*).

Overall Atructure—tGTPCH1 showed high stability at elevated temperatures (up to 95°C at pH 7.5) and a wide range of pH values (pH 5–11 at 25°C) (data not shown). By using this thermostable GTPCH1, high-quality crystals easily formed and high-resolution (2.2 Å) data were obtained (Table 1). The decamer structure is shown in Fig. 2, (a and b). Ten α-helices, one from each subunit, are arranged in tandem at the central core surrounded by a β-barrel. The active sites are situated between the β-sheet and the linker region for the α-helix: Cys108 and His111, from the β-turn, Cys179, from the β-sheet to the α-helix boundary, and a zinc ion form an active site with a distorted trigonal geometry (Fig. 2c). This zinc ion was confirmed by the X-ray absorption fine structure (*29*) (data not shown). The distances between the zinc ion and

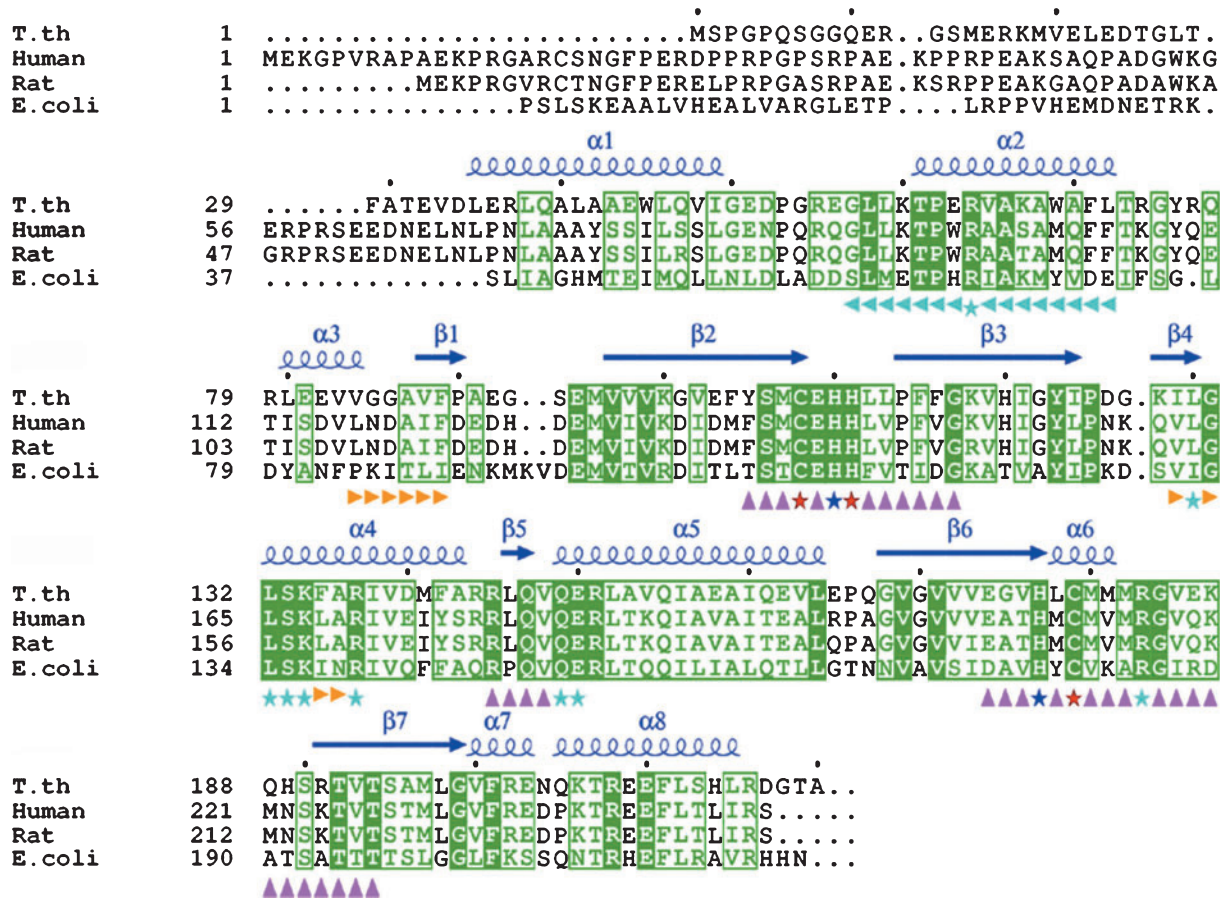

Fig. 3. **Amino acid sequences of GTPCH1s from various species.** Completely conserved residues are presented as white letters on a green background. Partially conserved residues are presented as green letters. Under the sequences, three red stars (Cys108, His111 and Cys179 of tGTPCH1) represent the residues coordinating directly to the zinc ion. The two blue stars represent the residues (His110 and His177 of tGTPCH1) participating in enzymatic catalysis. Cyan stars indicate the residues forming a hydrogen bond to the bound 8-oxo-GTP. Triangles represent the residues that form the ligand-binding pocket: magenta triangles represent the residues in one subunit forming the active site, orange triangles are the residues from the neighboring subunit, and cyan triangles are the residues on the opposite side of the subunit. The accession numbers for the amino acid sequences are GenBank S44049 for hGTPCH1, GenBank M58364 for rGTPCH1, and GenBank X63910 for eGTPCH1. This figure was created using ESPript (*20*).

the coordinating Sγ and Nδ atoms are 2.3–2.4 Å. These values are entirely consistent with those for other zinc-binding proteins (*31*). Several water molecules were found in the ligand-binding pocket. Based on five subunits per an asymmetrical unit, four water molecules were assigned to each active site. One water molecule (W2 in the A subunit, Fig. 2c) is 3.2 Å from the zinc ion on the opposite side of three coordinating residues. Another water molecule (W1 in Fig. 2c) forms a hydrogen bond with the Nε2 atom of His110, whereas another one (W3 in Fig. 2c) forms one wth the N atom of the Gln149 backbone. The fourth water molecule (W4 in Fig. 2c) forms a hydrogen bond with the Nη1 atom of Arg137 from the B subunit. These water molecules are likely to contribute to the substrate binding and transition state.

Structures of Complexes with 8-Oxoguanine Derivatives—The structures of tGTPCH1 complexed with 8-oxo-GTP and 8-oxo-dGTP, respectively, were determined at a resolution of 2.0 and 1.8 Å, respectively (Table 1). These high-resolution structures reveal details of the active site including the substrate analogue, zinc ion and water molecules (Fig. 4, a and b). As shown in Fig. 4a, the difference Fourier map (1Fo – Fc map, σ = 4.0) fits 8-oxo-GTP well. Both structures include one zinc ion and one 8-oxoguanine derivative per subunit. Two Sγ atoms from Cys108 and Cys179, the Nδ1 atom from His111, and the O8 atom from the 8-oxoguanine base are coordinated to the zinc ion in a tetrahedral geometry (Fig. 4, a and b). The average distances between the O8 atom of 8-oxoguanine and the zinc ion are 2.05 Å and 2.00 Å for 8-oxo-GTP and 8-oxo-dGTP, respectively.

The ribose conformation of bound nucleotides was found to be best represented by C1′ *exo* (*32*) in both complexes as a result of calculation by CNS (NMR and crystallography system, ver.1.1) (*33*) on refinement. However, in general, the ribose conformation of nucleosides or nucleotides is C2′ *endo*, C3′ *endo* or C3′ *exo* (*34*). Energy-minimization calculations indicated that the C2' *endo* conformation was possible for the ribose. Comparison of the C1′ *exo* form with the C2′ *endo* form on the difference Fourier map ($1F_o - F_c$ map) showed that the differences in the positions of individual atoms were too small to establish the ribose conformation with certainty at this resolution.

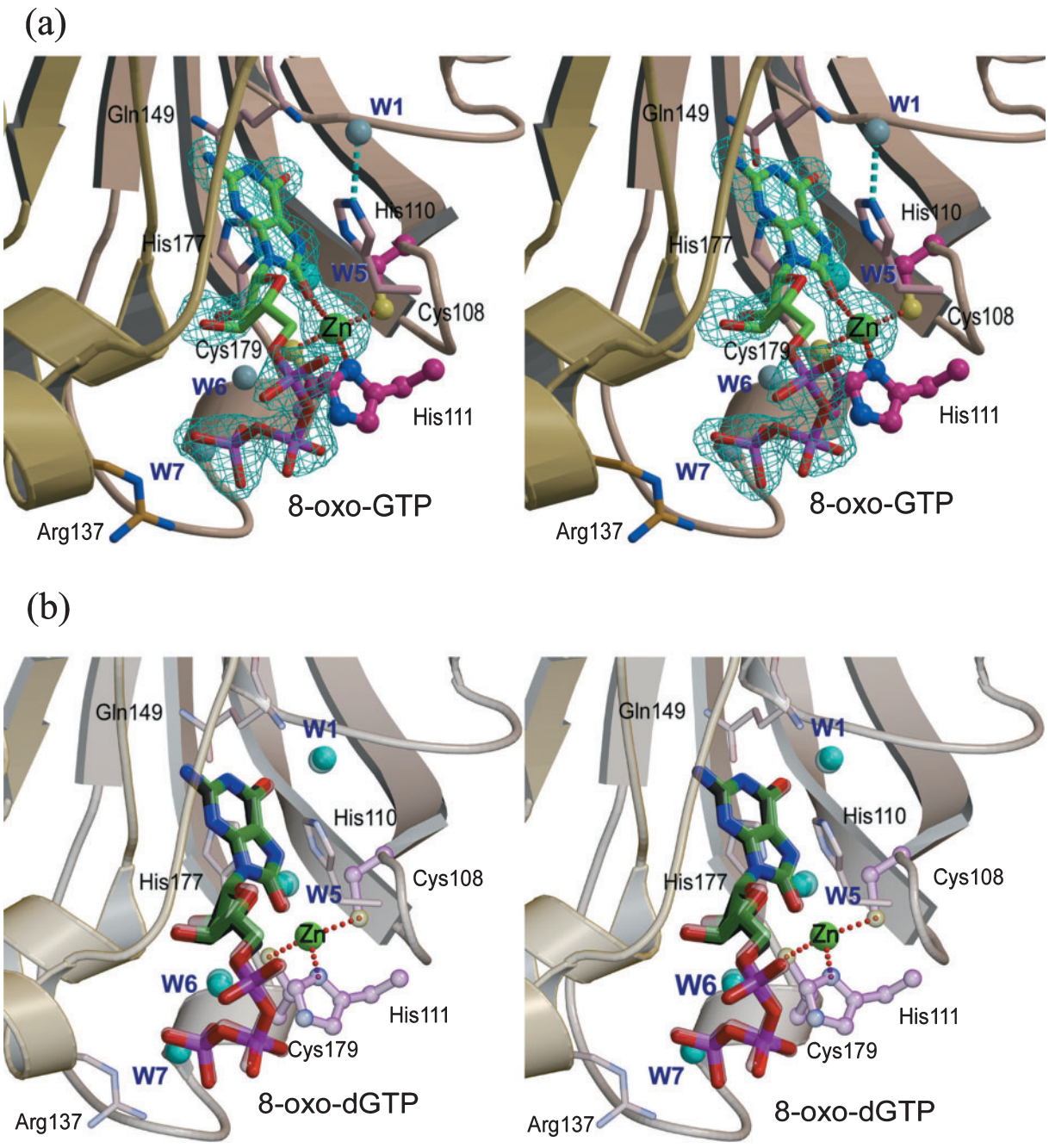

Fig. 4. **The binding mode of 8-oxo-GTP in the active site.** (a)W1 forms a hydrogen bond to His 110, whereas W5 forms hydrogen bonds to 8-oxo-GTP and His177. The difference Fourier map ($1\ F_o - F_c$ map, $\sigma = 4.0$) is superimposed on the model. (b) 8-oxo-dGTP (colored) can be exactly superimposed on 8-oxo-GTP (transparent) at the active site. Not only the bound ligands, but also the water molecules are consistent in both structures.

The substrate-binding pocket is formed from three adjacent subunits. The hydrogen-bond network around the active site is shown in Fig. 5. 8-Oxo-nucleotide binds to the protein like a wedge. The purine moiety is inserted into the protein, whereas the triphosphate moiety is bound near the pocket entrance. In this entrance region, there are three positively charged arginine residues (Arg64, Arg137 and Arg183) and one lysine residue (Lys134). The triphosphate moiety interacts with the positive charges in the binding pocket entrance. Part of the triphosphate moiety is also in contact with water molecules near the protein surface. In contrast, the ribose and purine moieties, which are inserted into the protein, are surrounded by neutral and hydrophobic residues. In particular, the residues that form the binding pocket from the neighboring subunit (Figs. 3 and 5) are hydrophobic in nature.

The bound ligand and the enzyme form 22 and 19 hydrogen bonds, either directly or through a water molecule, with the 8-oxo-GTP complex (Fig. 5) and 8-oxo-

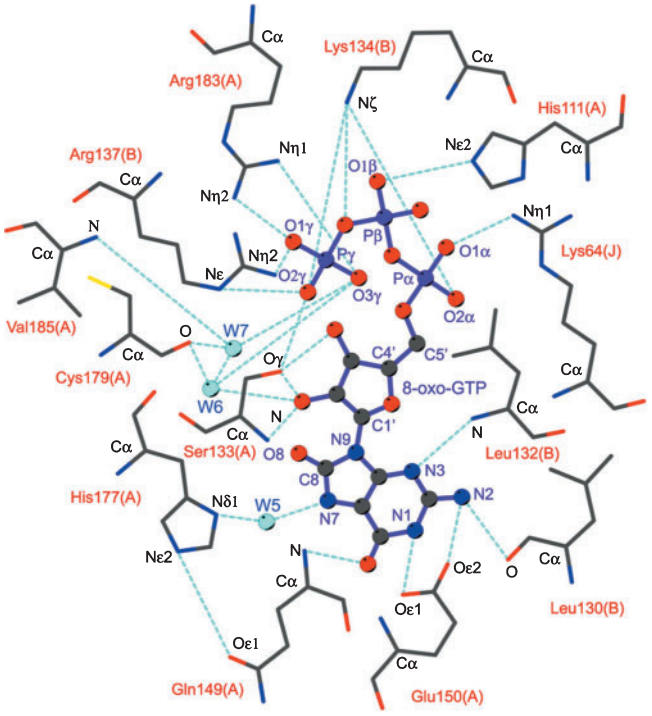

Fig. 5. **Schematic diagram of the hydrogen-bond network in the structure complexed with 8-oxo-GTP.** Dotted cyan lines indicate the hydrogen bonds. This figure was made with the LIGPLOT program (*21*)

dGTP complex (data not shown), respectively. For the 8-oxo-GTP complex the hydrogen bonding network can be divided as follows: 12 hydrogen bonds for the triphosphate moiety, 6 for the purine moiety, and 4 for the ribose moiety. In the case of 8-oxo-dGTP, which lacks the 2'-hydrolxyl group of the ribose, 3 hydrogen bonds are absent.

In the 8-oxo-GTP complex, at least 4 water molecules (*e.g.*, W1, W5, W6 and W7 in the A subunit, Fig. 4a) were identified from five active sites. One water molecule (W5) is positioned between the Nδ1 atom of His177 and the N-7 atom of the purine, distance 2.6 and 2.9 Å, respectively, which indicates the formation of hydrogen bonds to both atoms. One water molecule (W1) forms a hydrogen bond with the Nε2 atom of His110 on the opposite side of His110 from the zinc ion. This water molecule occupies the same location as in the free form (Figs. 2c and 4a). W6 and W7 form hydrogen bonds with the O atom of the Cys179 backbone. Compared with the structure of mutated eGTPCH1 [His113 (His111 in tGTPCH1) to Ser] complexed with GTP (*9*), the hydrogen bonding networks around the catalytically important water molecule (W5) and His177 were identified in tGTPCH1.

Superimpositioning of the free form on the complex with 8-oxo-GTP or 8-oxo-dGTP revealed significant alteration in the orientation of the imidazole ring plane of His110 and the benzene ring plane of Phe89 from the neighboring subunit (Fig. 6a). Compared with the free form, the imidazole rings were rotated by 41.5 and 58 degrees in the 8-oxo-GTP and 8-oxo-dGTP complexes, respectively. In the 8-oxo-GTP complex, the His110 imidazole ring plane faces the ribose O4′ atom in every subunit, whereas it points in the direction of the N9 atom of the purine moiety in the free enzyme. Rotation of the imidazole ring of His110 about the axis of the Cβ and C4 atoms is likely to be accompanied by the nearly simultaneous movement of the benzene ring of Phe89, which is probably caused by aromatic π–π interactions. Since the water molecule near His110 (W1 in the free form or W1 in the 8-oxo-GTP complex) is on the extended line of the Cβ-C4 axis (Figs. 2 and 4), this water molecule is unaffected by rotation of the imidazole ring.

In the 8-oxo-dGTP complex, however, in three of the five subunits (Fig. 6a), the imidazole ring of His110 points in the same direction as the free form (free-type), but in the other subunits (Fig. 6b), it points in the same direction as the 8-oxo-GTP complex (8-oxo-GTP-type). In the 8-oxo-dGTP-bound complex, the distances between the O4' atom of the ribose and the Nδ1 atom of His110 are 2.7 Å and 3.4 Å in the free-type and 8-oxo-GTP-type subunits, respectively (Fig. 6). A hydrogen bond can be formed when His 110 is in free-type state. This may imply the possible role of His110 in opening of the ribose in the course of the reaction catalyzed by GTPCH1.

DISCUSSION

8-Oxo-GTP as a Transition-State Inhibitor—During the course of our studies on nucleotide-related enzymes, we found that tGTPCH1 can tightly bind to 8-oxo-dGTP (Table 2). Furthermore, we determined the X-ray crystal structure of tGTPCH1 in a compelx with either 8-oxo-GTP or 8-oxo-dGTP together with a zinc ion, which ena-

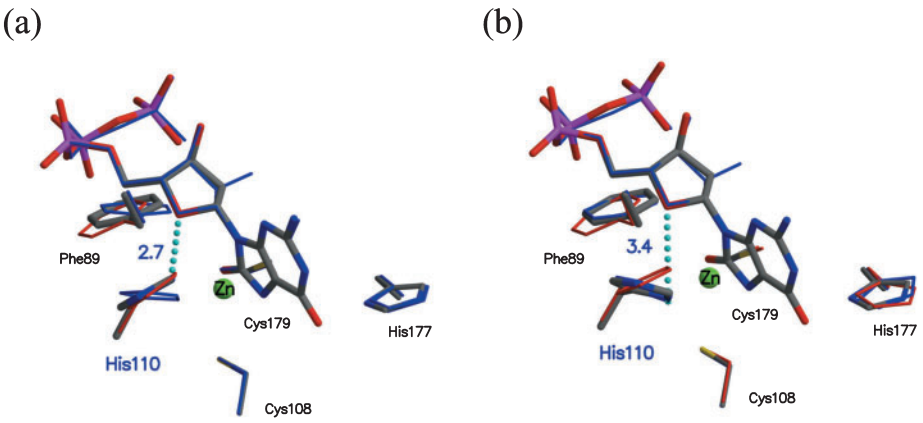

Fig. 6. **Rotation of the imidazole ring of His110.** The active sites of the free-type subunit (a) and 8-oxo-GTP-type (b) subunit are shown. Phe89, His110, Cys108, His177 and Cys179 of the free form are colored red. These residues and 8-oxo-GTP of the 8-oxo-GTP complex are colored blue. These residues and 8-oxo-dGTP of the 8-oxo-dGTP complex are represented in CPK colors.

bled us to analyze the reaction mechanism in detail, especially the reaction converting GTP to AFRPT. No structure of GTPCH1 complexed with zinc and GTP has been determined. Instead, a model structure was constructed by superimpositioning of two experimentally determined structures, one of the wild-type enzyme in the free form and the other of a mutant enzyme comprising zinc-chelating histidine complexed with GTP (*9*). Thus, this is the first report of a the ternary complex of GTPCH1, zinc and a GTP derivative.

A zinc ion is known to be important for purine ring opening (*7*). In the free form of tGTPCH1 (Fig. 2c), the zinc ion is coordinated by two S atoms from Cys108 and Cys109, and an N atom from His111. This coordination has also been observed for eGTPCH1 and hGTPCH1 (*7*). In the previously proposed mechanism (*7*), the zinc ion activates a water molecule near the C8 position of the purine ring to generate a hydroxyl nucleophile in close proximity to the imidazole ring of the bound substrate. One water molecule has been observed at a suitable position in the active site of eGTPCH1 (*7*). In this study, we identified the fixed water molecule (W2) situated near the zinc ion in the substrate-binding site. W2 is located too far (3.2 Å) from the zinc ion to be the fourth coordination position, and is not located on the line connecting the zinc and the guanine ring. There is a possibility, however, that when a substrate binds to the active site W2 changes its position and becomes the essential water molecule activated by the zinc ion. tGTPCH1 in complex with 8-oxo-GTP showed that the O8 atom is coordinated to the zinc ion, at a distance of 2.0 Å, at the fourth coordination position. In the proposed scheme (*7*), the zinc-bound hydroxyl ligand can then attack the C8 atom of the imidazole (see Fig. 7, I). Therefore, it is possible to envisage the O8 atom occupying the position where the oxygen of the hypothetical water molecule is located in the active site.

It should be remembered that 8-oxoguanine can exist in both keto and enol configurations of the C8 substitution (*35*). Unfortunately, X-ray crystallography cannot reveal the presence of hydrogen atoms methodologically. Theoretical calculation predicts that, as for the C8 position, the predominant species at neutral pH is the C8-keto form, along with protonated N7: the pK_a of the C8-enol has been determined to be ~12 (*36*). These data strongly suggest that the bound 8-oxo-GTP exists in the C8-keto configuration.

The interaction of GTPCH1 with many nucleotide derivatives (*23*, *25*, *37*), pteridine derivatives (*13*, *25*, *38–41*), and divalent metal ions (*23*, *42*) has been reported. However, the 8-oxoguanine derivatives of GTP have not been studied. It was only reported that the 8-oxoguanine base inhibited GTPCH1 activity, and that the affinity is much lower than that of 8-oxo-GTP (*43*). In this study, 8-oxo-GTP exhibited approximately 1,000-fold higher affinity for the enzyme over the substrate GTP. Furthermore, 8-oxo-(d)GTP was a very strong competitive inhibitor of the enzyme activity. Assuming the binding free energy is additive, the energetic contribution of each moiety to the affinity can be roughly estimated from the data in Table 2. The contribution of the 8-oxo group in the guanine base is –4 to –3 kcal/mol (*i.e.*, the energy difference ($\Delta\Delta G$) was –4.0 kcal/mol between GTP and 8-oxo-dGTP, and –2.7 kcal/mol between dGTP and 8-oxo-dGTP). The low affinity for the adenine base ($\Delta\Delta G$ was +1.6 kcal/mol between GTP and ATP) supports previous observations that GTPCH1 is specific for the guanine base. The contribution of the γ-phosphate group is 2.1 kcal/mol, and that of the 2′-OH group is 1 to 2 kcal/mol ($\Delta\Delta G$ was +0.9 kcal/mol between GTP and dGTP, and +2.2 kcal/mol between 8-oxo-GTP and 8-oxo-dGTP). These results indicate that the 8-oxo moiety of the guanine ring makes the greatest contribution to the observed affinity in comparison with other groups. Generally, transition state analogues show higher affinity for the enzyme than their respective substrates by 2–6 kcal/mol (*44–46*). Therefore, our kinetic results raise the possibility that an 8-oxoguanine derivative is one of the transition state analogues. The high affinity of the 8-oxo group for the active site supports at least the notion that the water molecule activated by the zinc ion attacks C8 of the substrate.

The reaction catalyzed by GTPCH1 comprises many elementary steps and is thus expected to involve many transition states. As shown in Fig. 1, AFRPT, the product generated on opening of the guanine ring, contains an oxygen atom at the C8 position. The apparent similarity of AFRPT to 8-oxo-GTP raises the possibility that 8-oxo-(d)GTP acts as an inhibitor analogous to AFRPT itself, not to a transition state. However, this possibility is unlikely because the NHCHO group cannot be located in the same plane as the base due to unfavorable steric clashing. This may be supported by the observation that the NHCHO group of cyclic 2,6-diamino-4-hydroxy-5-formamidopyrimidine (FapyG), which is structurally the same as the base moiety of AFRPT, is not in the plane of the base in the complex of MutM and a cyclic FapyG-containing DNA (*47*). The possibility is also unlikely that 8-oxo-GTP is an analogue of an intermediate between GTP and AFRPT (Fig. 7, III) because the steric configuration of the hydroxyl group at the C8 position differs from that of the 8-oxo group. Therefore, the most plausible explanation for the strong inhibition by 8-oxo-GTP is that the C8-keto form resembles a transition state intermediate in the course of AFRPT formation. Although a feasible configuration of the transition state is difficult to predict, a candidate for such an intermediate is that generated upon nucleophilic attack by the hydroxyl ion on GTP (Fig. 7, II).

Involvement of His177 in AFRPT Formation—In addition to the strong inhibitory effect of 8-oxoguanine, the structures determined in this study provide new insights into important aspects of enzymatic catalysis. Nucleophilic attack by a hydroxyl ion occurs at the N7-C8 bond of guanine, inevitably accompanied by protonation of the N7 atom (Fig. 7, II and III). In the 8-oxo-GTP bound forms, one water molecule (W5) lies in close proximity to N7 and the imidazole ring of His177. The bound 8-oxo-GTP exists in the C8-keto configuration with the N7 atom protonated, whereas the N7 atom is not protonated in GTP. If GTP and W5 bind to the active site in the same manner as in the 8-oxo-GTP bound form, the N7 atom can form a hydrogen bond with this water molecule in the ground state. Therefore, it is possible that W5 plays an important role in facilitating reduction of the double-bond between C8 and N7 by providing a proton to N7. No water molecule corresponding to W5 has been assigned

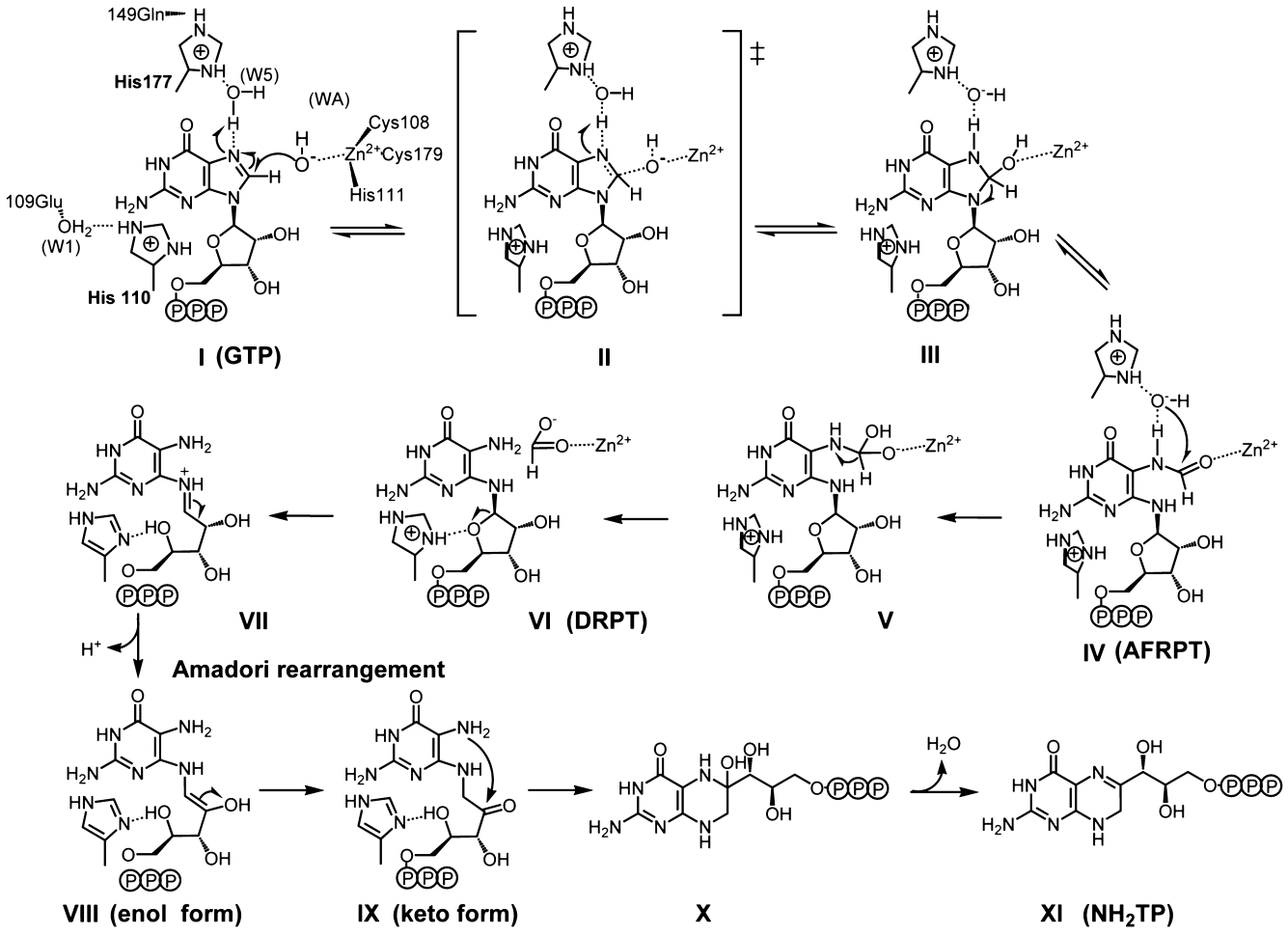

Fig. 7. **Proposed mechanism for the reaction catalyzed by GTPCH1.** Two water molecules (WA and W5) play important roles in holding the substrate and initiating the nucleophilic attack. His110 imidazole acts as a general acid on ribose ring opening. The details are given in the text.

previously, probably due to low resolution, and the previous models (*9*, *48*) assumed that the ring opening of the guanine base proceeds without such a water molecule. However, the presence of a fixed water molecule near N7 should increase the pK_a, thus promoting the protonation of N7 in the transition state, since the pK_a of N7 of the guanine is below 2 (*49*).

The W5 molecule may play a functional role also in cleavage of the formamide bond of AFRPT (Fig. 7, IV). The precise structure has not been determined for the AFRPT-bound form. However, it is probable that a water molecule corresponding to W5 is located at a similar position because W5 can also make a hydrogen bond with the Nδ1 atom of His177 (Fig. 5). His177 is completely conserved among GTPCH1s (Fig. 2), suggesting its important role in the reaction. eGTPCH1 mutants of His179, corresponding to His177 of tGTPCH1, accumulate AFRPT (Fig. 1), implying that this residue assists the cleavage of the formamide bond of AFRPT (*9*). Based on our structure, His177 seems to be required for activation of the water molecule for nucleophilic attack on AFRPT. Involvement of His177 in hydration of the formyl group via the water molecule can explain well the results of mutation studies (*9*). Alternatively, His177 may assist the precise location of the water molecule activated by the zinc ion (*9*), although no water molecule was detected at such a position in this study.

The Nε2 atom of the imidazole group of His177 can make a hydrogen bond with the oxygen atom of the side-chain amido group of Gln149 at a distance of 2.8 Å. The glutamine residue at this position is completely conserved (Fig. 2), and the interaction with the histidine is also conserved in the eGTPCH1 structure (the distance is 2.7 Å) (*9*). Therefore, the likely role of Gln149 is to fix the imidazole group in an appropriate position and orientation for catalysis. Gln149 may also affect the protonation state of Nε2 of His177 by keeping Nδ1 protonated.

Rotation of the Imidazole Ring of His110—The structure of the 8-oxo-dGTP complex is almost the same as that of the 8-oxo-GTP complex, except for one side chain, His110. The direction of the imizadole ring can be classified into the free-type and 8-oxo-GTP-type (Fig. 6). The two configurations of the pentamer structure suggest that the His110 imidazole ring can rotate between the free-type and the 8-oxo-GTP-type. In the free-type configuration, a hydrogen bond can form between His110 and the O4′ atom. The side-chain direction of His112 in the Cys181Ser mutant of eGTPCH1 (PDB code; 1N3T) is

similar to that of the 8-oxo-GTP-type of His110 in tGTPCH1, whereas that in free eGTPCH1 is similar to the free-type in tGTPCH1. The hydrogen-bond network is also similar between tGTPCH1 and eGTPCH1 (*9*). According to the proposed model (*9*), His112 in eGTPCH1 acts as a proton acceptor, rotates its imidazole group and then acts as a proton donor to transfer a proton to the ribose ring of GTP. In the case of tGTPCH1, however, there is no interaction between His110 and a ligand to the zinc ion. This seems inconsistent with the notion that His112 acts as a proton acceptor upon nucleophilic attack of the zinc-activated water. Instead, in our structures, the Nε2 atom of His110 can form a hydrogen bond with the W1 molecule (Fig. 4a). The W1 molecule is conserved in the three structures (Figs. 2c and 4b). The W1 molecule forms a hydrogen bond with the Oε2 atom of the carboxyl group of Glu109 at a distance of 2.7 Å. The side-chain carboxyl group of the conserved Glu109 residue (Fig. 3) may play a similar role to the amide group of Gln149 by fixing the position of His110 and maintaining its Nε2 atom in a protonated state *via* the W1 molecule.

Novel Reaction Mechanism—Based on these results, we propose a novel reaction mechanism for the early phase of the GTPCH1 reaction, as shown in Fig. 7. Upon conversion of GTP to AFRPT, the water molecule (WA) is activated by the zinc ion and makes a nucleophilic attack on the C8 atom of GTP to yield the tetrahedral transition state, which may resemble the 8-oxo-GTP complex structure (Figs. 6 and 7, II). N7 accepts the proton from the water molecule (W5) (III) and the C8-N9 bond is cleaved to produce AFRPT (IV). The reaction step from GTP to AFRPT is reversible and fast (*50*). The hydroxyl ion, formed as a result of the deprotonation of W5, nucleophilically attacks C8 to form another tetrahedral intermediate (V). The C8-N7 bond is cleaved to produce DRPT and the C8 atom is released as formic acid (VI). The released formic acid might coordinate to the zinc ion. During or after this release, the imidazole ring of His110 rotates, and a hydrogen bond between Nδ1 of His110 and O4′ of the ribose is formed to protonate Nδ1 (VI). 2,4-Diamino-5-formamidopyrimidine nucleotide, which is structurally similar to DRPT, can easily epimerize and the C1′-O4′ bond is cleaved spontaneously (*51*). However, the GTPCH1 reaction proceeds by two orders of magnitude faster than the epimerization rate of 2,4-diamino-5-formamidopyrimidine. In the case of GTPCH1, Nε2 of His110 could act as a general acid, yielding a Schiff base (VII). The hydrogen bond between Nδ1 and O4′ is maintained until product release. The Schiff base intermediate is converted to the enol form, which is spontaneously isomerized to the keto form (VIII and IX). The N7 atom could then nucleophilically attack C2′ to close the pteridine ring. The resulting dehydration generates NH_2TP (XI).

The pH profile of tGTPCH1 activity suggested that a functional group with a pK_a of about 6 participates in this reaction (data not shown). A histidine imidazole has a pK_a value of 6–7 and is thus a likely candidate. However, according to our model of the GTHCH1 reaction, His177 is active in the acid form, which contradicts the observed pH profile. For the same reason, His110 imidazole cannot be a candidate. The phosphate moiety of GTP also has a pK_a of around 6 (*52*). In addition, the pK_a value of the water molecule activated by the zinc ion is 6.2–6.9, as shown for carbonic anhydrase (*53*). Among these candidates, the ionizing state of the activated water molecule is most likely consistent with the observed pH profile.

There is considerable speculation concerning the later phase of the GTPCH1 reaction, including Amadori rearrangement, although the structures determined here provide no direct information about this part of the reaction. Compared with other enzymes catalyzing similar reactions, the keto-enol tautomerization might be rate-limiting and proceed nonenzymatically among the reaction steps of GTPCH1 including Amadori rearrangement and cyclization (*48*, *54*). However, the isomerization rates of the enzymes (~1 s^{-1}, pH 7.5, 25°C) (*55*) are much faster than the k_{cat} values of GTPCH1 (0.003–0.06 s^{-1}, pH 7.4–8.5, 37°C) (*12*, *25–28*, *54*, *56*). Therefore, the cyclization step might be rate-limiting in the GTPCH1 reaction. In addition, a large conformational change of the intermediate would be required for efficient attack on the carbohydrate chain by the N7 atom of the pyrimidone moiety (*57*). Molecular dynamic studies have suggested that the ring closure reaction requires distortion of the Michaelis-complex to optimize the geometry of the substrate (*58*). Direct involvement of several amino acid residues in such a drastic change is thought to be required for the pteridine ring closure. This may make the cyclization step rate-limiting.

Possible Physiological Meaning of High Affinity for 8-Oxo-GTP—8-Oxoguanine is a well-known oxidative product, and its incorporation into DNA causes mismatch base pairing. This type of mutation in DNA can result in degenerative diseases and cancer (*59*). For example, the level of 8-oxoguanine in DNA is elevated in the substantia nigra of Parkinson's disease brain (*60*). Although 8-oxoguanine can occur in free GTP and dGTP, apart from on DNA replication, the influence of this oxidation on cellular function has not been fully examined. In this study, 8-oxo-GTP and 8-oxo-dGTP strongly inhibited tGTPCH1 activity. This strong affinity of 8-oxoguanine derivatives is thought to be common to all GTPCH1s. GTPCH1 is the rate-limiting step in the *de novo* biosynthesis of BH_4. BH_4 serves as a cofactor of nitric oxide synthase (*61*) and enzymes involved in the biosynthetic pathways of several neurotransmitters, such as catecholamine and serotonin (*62*). If the concentration of 8-oxo-GTP were elevated, inhibition of GTPCH1 might lead to a decrease in the intracellular concentration of BH_4. Therefore, increased levels of 8-oxo-GTP may lead to arteriosclerosis or various neurotransmitter-related diseases (*e.g.*, Parkinson's disease, Alzheimer's disease, depression and autism) (*43*). Here, we examine the influence of 8-oxo-GTP on GTPCH1 function *in vivo*.

The GTP concentration is 150 μM in rat liver (*63*). The 8-oxoguanine/guanine ratios in normal cell DNA are $10.5/10^6$ in pig liver and $0.8–5.2/10^6$ in HeLa cells (*64*). When the ratio of $5.0:10^6$ is applied to free GTP/8-oxo-GTP, the 8-oxo-GTP concentration is assumed to be 0.75 nM. The GTPCH1 concentration in rat liver is 16 nM (*65*). In the presence of both GTP (S) and 8-oxo-GTP (I), GTPCH1 (E) can form an inhibitory complex (EI) as well as a Michaelis complex (ES). The ES complex to total enzyme complex ratio (α) was calculated with various levels of 8-oxoguanine/guanine (Table 3). With the 8-oxo-

Table 3. **The percentage of active enzyme-substrate complex.**

8-oxoguanine ratio	8-oxo-GTP (nM)	α (%)
0.000001	0.15	100.0
0.00001	1.5	99.6
0.0001	15	93.6
0.001	150	57.6
0.01	1500	11.5

The concentrations of GTPCH1 and GTP were assumed to be 16 nM and 150 μM, respectively. α is the ratio of intact enzyme-substrate complex to total enzyme complex.

guanine/guanine ratio of 0.000001, which has been reported for normal cells, GTPCH1 is almost unaffected by 8-oxo-GTP (α = 100). With the ratio of 0.001, which is near the ratio observed for Parkinson's disease or Alzheimer's disease brain (*60*, *66*), the α value reaches approximately 60%. Therefore, a 100 or 1,000-fold increase in the 8-oxo-GTP concentration could result in significant inhibition of GTPCH1 activity and subsequently cause severe aberrations in the biosynthesis of neurotransmitters. If this is the case, defense systems against guanine oxidation may act to protect cells not only from the mutagenic effects on genetic information but also from the physiological effect on metabolism *via* GTPCH1.

We wish to thank Drs. Y. Kawano and H. Nakajima for the assistance during the data collection at the SPring-8 synchrotron beam line, BL45XU–PX. We also thank Dr. A. Okamoto (Tokai University) for the useful advice on refinement.

REFERENCES

1. Shiota, T., Baugh, C.M., and Myrick, J. (1969) The assignment of structure to the formamidopyrimidine nucleoside triphosphate precursor of pteridines. *Biochim. Biophys. Acta* **192**, 205–210
2. Bracher, A., Fischer, M., Eisenreich, W., Ritz, H., Schramek, N., Boyle, P., Gentili, P., Huber, R., Nar, H., Auerbach, G., and Bacher, A. (1999) Histidine 179 mutants of GTP cyclohydrolase I catalyze the formation of 2-amino-5-formylamino-6-ribofuranosylamino-4(3H)-pyrimidinone triphosphate. *J. Biol. Chem.* **274**, 16727–16735
3. Burg, A.W. and Brown, G.M. (1968) The biosynthesis of folic acid. VIII. Purification and properties of the enzyme that catalyzes the production of formate from carbon atom 8 of guanosine triphosphate. *J. Biol. Chem.* **243**, 2349–2358
4. Wolf, W.A. and Brown, G.M. (1969) The biosynthesis of folic acid. X. Evidence for an Amadori rearrangement in the enzymatic formation of dihydroneopterin triphosphate from GTP. *Biochim. Biophys. Acta* **192**, 468–478
5. Bracher, A., Eisenreich, W., Schramek, N., Ritz, H., Gotze, E., Herrmann, A., Gutlich, M., and Bacher, A. (1998) Biosynthesis of pteridines. NMR studies on the reaction mechanisms of GTP cyclohydrolase I, pyruvoyltetrahydropterin synthase, and sepiapterin reductase. *J. Biol. Chem.* **273**, 28132–28141
6. Nar, H., Huber, R., Meining, W., Schmid, C., Weinkauf, S., and Bacher, A. (1995) Atomic structure of GTP cyclohydrolase I. *Structure* **3**, 459–466
7. Auerbach, G., Herrmann, A., Bracher, A., Bader, G., Gutlich, M., Fischer, M., Neukamm, M., Garrido-Franco, M., Richardson, J., Nar, H., Huber, R., and Bacher, A. (2000) Zinc plays a key role in human and bacterial GTP cyclohydrolase I. *Proc. Natl Acad. Sci. USA* **97**, 13567–13572
8. Nar, H., Huber, R., Auerbach, G., Fischer, M., Hosl, C., Ritz, H., Bracher, A., Meining, W., Eberhardt, S., and Bacher, A. (1995) Active site topology and reaction mechanism of GTP cyclohydrolase I. *Proc. Natl Acad. Sci. USA* **92**, 12120–12125
9. Rebelo, J., Auerbach, G., Bader, G., Bracher, A., Nar, H., Hosl, C., Schramek, N., Kaiser, J., Bacher, A., Huber, R., and Fischer, M. (2003) Biosynthesis of pteridines. Reaction mechanism of GTP cyclohydrolase I. *J. Mol. Biol.* **326**, 503–516
10. Oshima, T. and Imahori, K. (1974) Description of *Thermus thermophilus* (Yoshida and Oshima) comb. nov., a onsporulating thermophilic bacterium from a Japanese thermal spa. *Int. J. Syst. Bacteriol.* **24**, 102–112
11. Yokoyama, S., Hirota, H., Kigawa, T., Yabuki, T., Shirouzu, M., Terada, T., Ito, Y., Matsuo, Y., Kuroda, Y., Nishimura, Y., Kyogoku, Y., Miki, K., Masui, R., and Kuramitsu, S. (2000) Structural genomics projects in Japan. *Nat. Struct. Biol.* **7 Suppl**, 943–945
12. Fukushima, K., Richter, W.E., Jr., and Shiota, T. (1977) Partial purification of 6-(D-erythro-1′,2′,3′-trihydroxypropyl)-7,8-dihydropterin triphosphate synthetase from chicken liver. *J. Biol. Chem.* **252**, 5750–5755
13. Hatakeyama, K., Inoue, Y., Harada, T., and Kagamiyama, H. (1991) Cloning and sequencing of cDNA encoding rat GTP cyclohydrolase I. The first enzyme of the tetrahydrobiopterin biosynthetic pathway. *J. Biol. Chem.* **266**, 765–769
14. Fersht, A. (1999) *Structure and Mechanism in Protein Sci.: A Guide to Enzyme Catalysis and Protein Folding*, WH. Freeman and Co., New York
15. Watanabe, R., Masui, R., Mikawa, T., Takamatsu, S., Kato, R., and Kuramitsu, S. (1994) Interaction of *Escherichia coli* RecA protein with ATP and its analogues. *J. Biochem.* **116**, 960–966
16. Otwinowski, Z. and Minor, W. (1997) Processing of x-ray diffraction data collected in oscillation mode. *Methods Enzymol.* **276**, 307–326
17. Navaza, J. (1994) AMoRe: an automated package for molecular replacement. *Acta Crystallogr. A* **50**, 157–163
18. Kraulis, P.J. (1991) MOLSCRIPT: a program to produce both detailed and schematic plots of protein structures. *J. Appl. Crystallogr.* **24**, 946–950
19. Merritt, E.A. and Murphy, M.E.P. (1994) Raster3D Version 2.0. A program for photorealistic molecular graphics. *Acta Crystallog. sect. D* **50**, 869–873
20. Gouet, P., Courcelle, E., Stuart, D.I., and Metoz, F. (1999) ESPript: analysis of multiple sequence alignments in postscript. *Bioinformatics* **15**, 305–308
21. Wallace, A.C., Laskowski, R.A., and Thornton, J.M. (1995) LIGPLOT: a program to generate schematic diagrams of protein-ligand interactions. *Protein Eng.* **8**, 127–134
22. Kuramitsu, S., Hiromi, K., Hayashi, H., Morino, Y., and Kagamiyama, H. (1990) Pre-steady-state kinetics of *Escherichia coli* aspartate aminotransferase catalyzed reactions and thermodynamic aspects of its substrate specificity. *Biochemistry* **29**, 5469–5476
23. Weisberg, E.P. and O'Donnell, J.M. (1986) Purification and characterization of GTP cyclohydrolase I from *Drosophila melanogaster*. *J. Biol. Chem.* **261**, 1453–1458
24. Schoedon, G., Redweik, U., and Curtius, H.C. (1989) Purification of GTP cyclohydrolase I from human liver and production of specific monoclonal antibodies. *Eur. J. Biochem.* **178**, 627–634
25. Hatakeyama, K., Harada, T., Suzuki, S., Watanabe, Y., and Kagamiyama, H. (1989) Purification and characterization of rat liver GTP cyclohydrolase I. Cooperative binding of GTP to the enzyme. *J. Biol. Chem.* **264**, 21660–21664
26. WIitter, K., Cahill, J.C., Werner, T., Ziegler, I., Rodl, W., Bacher, A., and Gutlich, M. (1996) Molecular cloning of a cDNA coding for GTP cyclohydrolase I from *Dictyostelium discoideum*. *Biochem. J.* **319**, 27–32
27. He, A., Simpson, D.R., Daniels, L., and Rosazza, J.P. (2004) Cloning, expression, purification, and characterization of *Nocardia* sp. GTP cyclohydrolase I. *Protein Expr. Purif.* **35**, 171–180
28. Suzuki, T., Kurita, H., and Ichinose, H. (2004) GTP cyclohydrolase I utilizes metal-free GTP as its substrate. *Eur. J. Biochem.* **271**, 349–355

29. Maita, N., Okada, K., Hatakeyama, K., and Hakoshima, T. (2002) Crystal structure of the stimulatory complex of GTP cyclohydrolase I and its feedback regulatory protein GFRP. *Proc. Natl Acad. Sci. USA* **29**, 1212–1217
30. Szilagyi, A. and Zavodszky, P. (2000) Structural differences between mesophilic, moderately thermophilic and extremely thermophilic protein subunits: results of a comprehensive survey. *Structure* **8**, 493–504
31. Lipscomb, W.N. and Strater, N. (1996) Recent advances in zinc enzymology. *Chem. Rev.* **96**, 2375–2434
32. Koepke, J., Maslowska, M., Heinemann, U., and Saenger, W. (1989) Three-dimensional structure of ribonuclease T1 complexed with guanylyl-2′,5′-guanosine at 1.8 Å resolution. *J. Mol. Biol.* **206**, 475–488
33. Brunger, A.T., Adams, P.D., Clore, G.M., DeLano, W.L., Gros, P., Grosse-Kunstleve, R.W., Jiang, J.S., Kuszewski, J., Nilges, M., Pannu, N.S., Read, R.J., Rice, L.M., Simonson, T., and Warren, G.L. (1998) Crystallography & NMR system: A new software suite for macromolecular structure determination. *Acta Crystallogr. D* **54**, 905–921
34. Sundaralingam, M. (1969) Stereochemistry of nucleic acids and their constituents. IV. Allowed and preferred conformations of nucleosides, nucleoside mono-, di-, tri-, tetraphosphates, nucleic acids and polynucleotide. *Biopolymers* **7**, 821–860
35. Kouchakdjian, M., Bodepudi, V., Shibutani, S., Eisenberg, M., Johnson, F., Grollman, A.P., and Patel, D.J. (1991) NMR structural studies of the ionizing radiation adduct 7-hydro-8-oxodeoxyguanosine (8-oxo-7H-dG) opposite deoxyadenosine in a DNA duplex. 8-Oxo-7H-dG(syn).dA(anti) alignment at lesion site. *Biochemistry* **30**, 1403–1412
36. Culp, S.J., Cho, B.P., Kadlubar, F.F., and Evans, F.E. (1989) Structural and conformational analyses of 8-hydroxy-2′-deoxyguanosine. *Chem. Res. Toxicol.* **2**, 416–422
37. Yim, J.J. and Brown, G.M. (1976) Characteristics of guanosine triphosphate cyclohydrolase I purified from *Escherichia coli*. *J. Biol. Chem.* **251**, 5087–5094
38. Schoedon, G., Redweik, U., Frank, G., Cotton, R.G., and Blau, N. (1992) Allosteric characteristics of GTP cyclohydrolase I from *Escherichia coli*. *Eur. J. Biochem.* **210**, 561–568
39. Shen, R.S., Alam, A., and Zhang, Y.X. (1988) Inhibition of GTP cyclohydrolase I by pterins. *Biochim. Biophys. Acta* **965**, 9–15
40. Sung, Y.J., Hotchkiss, J.H., and Dietert, R.R. (1994) 2,4-Diamino-6-hydroxypyrimidine, an inhibitor of GTP cyclohydrolase I, suppresses nitric oxide production by chicken macrophages. *Int. J. Immunopharmacol.* **16**, 101–108
41. Bellahgense, Z., Dhondt, J., and farrioaux, J. (1984) Guanosine triphosphate cyclohydrolase activity in rat tissues. *Biochem. J.* **217**, 59–65
42. Cha, K.W., Jacobson, K.B., and Yim, J.J. (1991) Isolation and characterization of GTP cyclohydrolase I from mouse liver. Comparison of normal and the hph-1 mutant. *J. Biol. Chem.* **266**, 12294–12300
43. Yoneyama, T., Wilson, L.M., and Hatakeyama, K. (2001) GTP cyclohydrolase I feedback regulatory protein-dependent and -independent inhibitors of GTP cyclohydrolase I. *Arch. Biochem. Biophys.* **388**, 67–73
44. Secemski, I.I, Lehrer, S.S., and Lienhard, G.E. (1972) A transition state analog for lysozyme. *J. Biol. Chem.* **247**, 4740–4748
45. Qasim, M.A., Lu, S.M., Ding, J., Bateman, K.S., James, M.N., Anderson, S., Song, J., Markley, J.L., Ganz, P.J., Saunders, C.W., and Laskowski, M., Jr. (1999) Thermodynamic criterion for the conformation of P1 residues of substrates and of inhibitors in complexes with serine proteinases. *Biochemistry* **38**, 7142–7150
46. Wolfenden, R. (1972) Analogue approaches to the structure of the transition state in enzyme reactions. *Acc. Chem. Res.* **5**, 10–18
47. Coste, F., Ober, M., Carell, T., Boiteux, S., Zelwer, C., and Castaing, B. (2004) Structural basis for the recognition of the FapydG lesion (2,6-diamino-4-hydroxy-5-formamidopyrimidine) by formamidopyrimidine-DNA glycosylase. *J. Biol. Chem.* **279**, 44074–44083
48. Bracher, A., Schramek, N., and Bacher, A. (2001) Biosynthesis of pteridines. Stopped-flow kinetic analysis of GTP cyclohydrolase I. *Biochemistry* **40**, 7896–7902
49. Saenger, W. (1984) *Principles of Nucleic Acid Structure*, Springer Verlag New York, New York
50. Schramek, N., Bracher, A., Fischer, M., Auerbach, G., Nar, H., Huber, R., and Bacher, A. (2002) Reaction mechanism of GTP cyclohydrolase I: single turnover experiments using a kinetically competent reaction intermediate. *J. Mol. Biol.* **316**, 829–837
51. Greenberg, M.M., Hantosi, Z., Wiederholt, C.J., and Rithner, C.D. (2001) Studies on N4-(2-deoxy-D-pentofuranosyl)-4,6-diamino-5-formamidopyrimidine (Fapy.dA) and N6-(2-deoxy-D-pentofuranosyl)-6-diamino-5-formamido-4-hydroxypyrimidine (Fapy.dG). *Biochemistry* **40**, 15856–15861
52. Bock, R.M., Ling, N.S., Morell, S.A., and Lipton, S.H. (1956) Ultraviolet absorption spectra of adenosine-5′-triphosphate and related 5′-ribonucleotides. *Arch. Biochem. Biophys.* **62**, 253–264
53. Baird, T.T., Jr., Waheed, A., Okuyama, T., Sly, W.S., and Fierke, C.A. (1997) Catalysis and inhibition of human carbonic anhydrase IV. *Biochemistry* **36**, 2669–2678
54. Schramek, N., Bracher, A., and Bacher, A. (2001) Ring opening is not rate limiting in the GTP cyclohydrolase I reaction. *J. Biol. Chem.* **276**, 2622–2626
55. Eberhard, M., Tsai-Pflugfelder, M., Bolewska, K., Hommel, U., and Kirschner, K. (1995) Indoleglycerol phosphate synthase-phosphoribosyl anthranilate isomerase: comparison of the bifunctional enzyme from *Escherichia coli* with engineered monofunctional domains. *Biochemistry* **34**, 5419–5428
56. De Saizieu, A., Vankan, P., and van Loon, A.P. (1995) Enzymic characterization of *Bacillus subtilis* GTP cyclohydrolase I. Evidence for a chemical dephosphorylation of dihydroneopterin triphosphate. *Biochem. J.* **306**, 371–377
57. Wei, C.C., Crane, B.R. and Stuehr, D.J. (2003) Tetrahydrobiopterin radical enzymology. *Chem. Rev.* **103**, 2365–2383
58. Mazumder-Shivakumar, D. and Bruice, T.C. (2004) Molecular dynamics studies of ground state and intermediate of the hyperthermophilic indole-3-glycerol phosphate synthase. *Proc. Natl Acad. Sci. USA* **101**, 14379–14384
59. Bruner, S.D., Norman, D.P., Fromme, J.C., and Verdine, G.L. (2000) Structural and mechanistic studies on repair of 8-oxoguanine in mammalian cells. *Cold Spring Harb. Symp. Quant. Biol.* **65**, 103–111
60. Alam, Z.I., Jenner, A., Daniel, S.E., Lees, A.J., Cairns, N., Marsden, C.D., Jenner, P., and Halliwell, B. (1997) Oxidative DNA damage in the parkinsonian brain: an apparent selective increase in 8-hydroxyguanine levels in substantia nigra. *J. Neurochem.* **69**, 1196–1203
61. Reif, D.W. and McCreedy, S.A. (1995) N-nitro-L-arginine and N-monomethyl-L-arginine exhibit a different pattern of inactivation toward the three nitric oxide synthases. *Arch. Biochem. Biophys.* **320**, 170–176
62. Kaufman, S. (1987) Aromatic amino acid hydroxylases in *The Enzymes*, 3rd ed. (Boyer, P.D. and Krebs, E.G., eds.) Vol. **18**, pp. 217–282, Academic Press, New York
63. Greengard, O. and Delvalle, J.A. (1976) The regulation of phenylalanine hydroxylase in rat tissues in vivo. Substrate- and cortisol-induced elevations in phenylalanine hydroxylase activity. *Biochem. J.* **154**, 619–624
64. ESCODD (2002) Comparative analysis of baseline 8-oxo-7, 8-dihydroguanine in mammalian cell DNA, by different methods in different laboratories: an approach to consensus. *Carcinogenesis* **23**, 2129–2133
65. Harada, T., Kagamiyama, H., and Hatakeyama, K. (1993) Feedback regulation mechanisms for the control of GTP cyclohydrolase I activity. *Science* **260**, 1507–1510
66. Gabbita, S.P., Lovell, M.A., and Markesbery, W.R. (1998) Increased nuclear DNA oxidation in the brain in Alzheimer's disease. *J. Neurochem.* **71**, 2034–2040